AD-A100 418 CINCINNATI UNIV OH DEPT OF MATERIALS SCIENCE AND MET--ETC F/G 12/1
EXAMINATION OF ERRORS IN THE DETERMINATION OF PHASE BOUNDARY TH--ETC(U)
JUN 81 R ROE N00014-77-C-0376
UNCLASSIFIED TR-6 NL

1 OF 1
AD A
100418

END
DATE
FILMED
7-81
DTIC

LEVEL II

AD A100418

SECURITY CLASSIFICATION OF THIS PAGE (When Data Entered)

REPORT DOCUMENTATION PAGE

READ INSTRUCTIONS BEFORE COMPLETING FORM

1. REPORT NUMBER: Technical Report No. 6

2. GOVT ACCESSION NO.: A100418

3. RECIPIENT'S CATALOG NUMBER: TR-6

4. TITLE (and Subtitle): Examination of Errors in the Determination of Phase Boundary Thickness by Small Angle X-ray Scattering

5. TYPE OF REPORT & PERIOD COVERED: Technical Report

6. PERFORMING ORG. REPORT NUMBER:

7. AUTHOR(s): Ryong-Joon Roe

8. CONTRACT OR GRANT NUMBER(s): N00014-77-C0326

9. PERFORMING ORGANIZATION NAME AND ADDRESS: Dept. of Materials Sci. & Metallurgical Engineering, M.L. #12, University of Cincinnati, Cincinnati, OH 45221

10. PROGRAM ELEMENT, PROJECT, TASK AREA & WORK UNIT NUMBERS: NR-356-655

11. CONTROLLING OFFICE NAME AND ADDRESS:

12. REPORT DATE: June 10, 1981

13. NUMBER OF PAGES: 31

14. MONITORING AGENCY NAME & ADDRESS (if different from Controlling Office):

15. SECURITY CLASS. (of this report):

15a. DECLASSIFICATION/DOWNGRADING SCHEDULE:

16. DISTRIBUTION STATEMENT (of this Report)

Approved for Public Release; distribution unlimited

17. DISTRIBUTION STATEMENT (of the abstract entered in Block 20, if different from Report)

DTIC ELECTE JUN 22 1981 E

18. SUPPLEMENTARY NOTES

19. KEY WORDS (Continue on reverse side if necessary and identify by block number)

Small-angle X-ray scattering, diffuse phase boundary thickness, errors

20. ABSTRACT (Continue on reverse side if necessary and identify by block number)

The method of determining the thickness of diffuse phase boundary with density profile governed by equilibrium conditions is proposed. It follows the well-known procedure of analyzing the deviations from Porod's law. Errors in the obtained boundary thickness, due to the statistical scatter in the intensity data and to the difficulty of separating

(over)

DD FORM 1 JAN 73 1473 EDITION OF 1 NOV 65 IS OBSOLETE

S/N 0102-LF-014-6601

SECURITY CLASSIFICATION OF THIS PAGE (When Data Entered)

(Abstract cont'd from block 20)

the effect of density fluctuations within the phases, are examined. For this purpose, scattering curves are synthesized on the basis of a well-defined model structure with known boundary thicknesses. These synthesized curves, when analyzed according to the proposed method, yield the correct boundary thickness under favorable conditions, but are also shown to lead to very erroneous results in some cases.

Accession For
NTIS GRA&I
DTIC TAB
Unannounced
Justification
By
Distribution/
Availability Codes
Avail and/or
Dist Special
A

OFFICE OF NAVAL RESEARCH

Contract N00014-77-C-0376

Task No. NR 356-655

TECHNICAL REPORT NO. 6

Examination of Errors in the Determination of Phase Boundary Thickness by Small Angle X-ray Scattering

by

Ryong-Joon Roe

Department of Materials Science and
Metallurgical Engineering
University of Cincinnati
Cincinnati, OH 45221

Prepared for Publication
in J. Appl. Cryst.

June 10, 1981

Reproduction in whole or in part is permitted for any purpose of the United States Government

This document has been approved for public release and sale; its distribution is unlimited

Abstract

The method of determining the thickness of diffuse phase boundary with density profile governed by equilibrium conditions is proposed. It follows the well-known procedure of analyzing the deviations from Porod's law. Errors in the obtained boundary thickness, due to the statistical scatter in the intensity data and to the difficulty of separating the effect of density fluctuations within the phases, are examined. For this purpose, scattering curves are synthesized on the basis of a well-defined model structure with known boundary thicknesses. These synthesized curves, when analyzed according to the proposed method, yield the correct boundary thickness under favorable conditions, but are also shown to lead to very erroneous results in some cases.

I. Introduction

The intensity of small-angle X-ray scattering (SAXS) by isotropic materials having ideal two phase structure decreases as s^{-4} at large s ($s = 2\sin\Theta/\lambda$), according to the theory by Porod (1951, 1952a, b). Deviations from this Porod law can occur in practice since the boundaries between the phases may not be perfectly sharp, and the electron densities within the phases contain local fluctuations. The potential utility of determining the phase boundary thickness, by examination of the deviation of observed SAXS intensity from Porod's law, was first pointed out by Ruland (1971) and was since examined by a number of workers (Vonk 1973; Ruland 1974; Hashimoto, Todo, Itoi and Kawai 1977; Todo, Hashimoto and Kawai 1978; Hashimoto, Shibayama and Kawai 1980; Koberstein, Morra and Stein 1980; Roe, Fishkis and Chang 1981).

According to Ruland (1971), the observed intensity $I_{obs}(s)$ can be expressed as

$$I_{obs}(s) = I_{id}(s)H^2(s) + I_b \qquad (1)$$

where $I_{id}(s)$ is the intensity due to ideal two phase structure, $H^2(s)$ is the factor arising from diffuseness of the boundaries, and I_b is the 'background' intensity due to local electron-density fluctuation within the phases. If the electron-density profile across the boundary approximates a convolution product of a step function and a gaussian function, $H^2(s)$ takes the form

$$H^2(s) = \exp(-4\pi^2\sigma^2 s^2) \qquad \text{(gaussian)} \qquad (2)$$

where the variance σ^2 of the gaussian function embodies the diffuseness of the boundary. Statistical-mechanical studies of inhomogeneous liquid systems (Cahn and Hilliard 1958), polymer mixtures

(Helfand and Tagami 1971; Hopper and Uhlmann 1974; Roe 1975) and block copolymers (Helfand 1975) showed that the density profile across the phase boundary attained under equilibrium conditions is given by

$$q(x) = \tanh(\pi x/\sqrt{12}\,\sigma) \tag{3}$$

In this case the corresponding $H^2(s)$ function is (Ruland 1980; Roe, Fishkis and Chang 1981)

$$H^2(s) = (\sqrt{12}\pi\sigma s)^2 \operatorname{csch}^2(\sqrt{12}\pi\sigma s) \quad \text{(equilibrium)} \tag{4}$$

The boundary thickness (or the value of σ) is determined by analysing the observed intensity in the Porod's region according to eq. (1), and for this purpose a suitable graphical or numerical method has to be devised. The simplest is to expand $H^2(s)$ in a series and retain the first two terms only. Koberstein, Morra and Stein (1980) showed that such a procedure is likely to lead to an underestimate of σ when the analysis is performed over a range of s in which truncation of higher order terms is not justified. They instead proposed a procedure, applicable when $H^2(s)$ is given by eq. (2), which is valid even for s greatly exceeding $1/\sigma$. One of the purposes of the present work is to present a similar procedure which is applicable when $H^2(s)$ is given by eq. (4) instead of eq. (2).

The main practical difficulty in utilizing eq. (1) for estimation of σ arises from uncertainties introduced by the errors in the observed data. The effect of diffuse boundaries, represented by $H^2(s)$, introduces a negative deviation from Porod's law, while the 'background' I_b contributes a positive deviation. These two effects therefore tend to cancel each other, and meaningful separation of one from the other is often found difficult because of

the statistical error in the data, which in the Porod's region is usually appreciable. It is desirable to have an estimate of the error in the evaluated σ value arising in practice as a result of the statistical error in the data. For this purpose in this work a series of 'theoretical' scattering curves based on a model structure are constructed, and are then given random statistical fluctuations to make them simulate experimentally determined data. These synthesized scattering curves are thereafter analyzed by the method proposed for the determination of σ values, and the values thus obtained are compared with the values initially chosen for the synthesized curves.

II. Procedure Applicable to Equilibrium Boundary Profile

When SAXS data are collected with instruments having slit collimation, the effect of the slit-smearing has to be properly taken into account. Because of the possible amplification of the error in the data in the process of desmearing, the procedure for the determination of the boundary thickness should preferably make use of the smeared data directly. The slit-smeared intensity $\tilde{I}(s)$ is given by

$$\tilde{I}(S) = 2\int_0^\infty W_\ell(u)\ I_{obs}(\sqrt{s^2+u^2})\ du \tag{5}$$

where $W_\ell(u)$ is the slit-length weighting function. In what follows, we will consider only the cases in which the infinite-slit approximation is valid. $W_\ell(u)$ is then a constant independent of u.

The intensity of ideal two phase structure in the Porod's region is given by

$$I_{id}(s) = (\Delta\rho)^2 S/8\pi^3 s^4 \tag{6}$$

where $\Delta\rho$ is the difference in the electron density between the two phases and S is the total phase boundary area. For the density profile across the phase boundary determined by equilibrium conditions, $H^2(s)$ is given by eq. (4), and therefore the slit-smeared intensity in the Porod's region can be written as

$$\tilde{I}(s) = A\tilde{g}(x) + \tilde{I}_b \tag{7}$$

where $\tilde{I}_b$ is the smeared 'background' intensity, and

$$A = 36\pi S(\Delta\rho)^2 W_\ell(0)\sigma^4 \tag{8}$$

$$x = \sqrt{12}\pi\sigma s \tag{9}$$

$$g(x) = \operatorname{csch}^2(x)/x^2 \tag{10}$$

$$\tilde{g}(x) = \int_0^\infty g(\sqrt{x^2+u^2})\, du \tag{11}$$

The integration indicated in eq. (11) could not be evaluated analytically, and in this work $\tilde{g}(x)$ was calculated numerically. For x between 0.8 and 6.0, $\tilde{g}(x)$ is approximated well by

$$\tilde{g}(x) \approx 3.3x^{-1.8}e^{-1.9x} \tag{12}$$

The root-mean-square error of this approximation over the above-mentioned range of x is 2% and the maximum error at the two ends of the range is 4%. Fig. 1 shows the plot of $\ln[x^{1.8}\tilde{g}(x)]$ against x, illustrating the good linearity in the indicated range of x.

Evaluation of σ from the observed intensity $\tilde{I}(s)$ would then proceed as follows. A plot of $\ln[\{\tilde{I}(s) - \tilde{I}_b\}s^{1.8}]$ against s is constructed, and the slope of the linear portion of the plot is determined. The value of σ is then given by

$$\sigma = -\text{slope}/(1.9\sqrt{12}\pi) \tag{13}$$

Alternatively, one could evaluate the effective thickness t by

$$t = -\text{slope}(2/1.9\pi^2) \tag{14}$$

where t, defined as the reciprocal of the density gradient at the center of the boundary layer, is related to σ by

$$t = (4\sqrt{3}/\pi)\sigma. \tag{15}$$

After σ has been evaluated, one may calculate x by eq. (9) to see whether the approximation (12) is justified in the range of s at which the slope was evaluated. In the (unlikely) event

that the x range starts at a value smaller than 0.8, the following alternative approximation may be employed.

$$\tilde{g}(x) \approx 2.0x^{-2.5}e^{-1.4x} \tag{16}$$

Eq. (16) is valid for x between 0.3 and 2.1, with the root-mean-square error equal to 2% and the maximum error equal to 4%. The required plot is then $\ln[\{\tilde{I}(s) - \bar{I}_b\}s^{2.5}]$ against s.

III. Synthesized Scattering Curves

It would be a difficult task to derive an analytical expression, in general terms, for the propagation of error from the initial data to the final σ value obtained. Instead, we take a simpler approach of synthesizing a model scattering curve and then applying the proposed procedure to it to see how closely the known σ value is recovered. In constructing the model scattering curves, effort is given to make them as realistic as possible. The physical constants required for their calculation are given values typically found in real systems of interest.

Two types of scattering curves are constructed. In the first, the model structure assumed is one in which spherical particles of one phase are imbedded in a continuous matrix of another phase, with the boundary between the phases given a predefined diffuseness. The second corresponds to a scattering from a single-phase two-components system. This is to examine what erroneous σ values are likely to be obtained when the system actually contains no two phase structure at all.

A. Structure containing spherical particles

Construction of the scattering curves proceeds in three stages:

deriving the scattering curve for pin-hole collimation, applying the slit smearing and adding random statistical error.

For an ideal two phase system containing spherical particles, of radius a distributed according to a distribution function w(a), the scattered intensity per unit volume of the sample is

$$I_{id}(s) = (\Delta\rho)^2 f_1 \int \phi^2(s,a) w(a) da / \int (4/3)\pi a^3 w(a) da \qquad (17)$$

where f_1 is the volume fraction of the spheres, and $\phi^2(s,a)$ represents the scattering from a sphere of radius a, given (Guinier 1963) by

$$\phi(s,a) = (4/3)\pi a^3 U(2\pi sa) \qquad (18)$$

$$U(x) = (3/x^3)(\sin x - x\cos x) \qquad (19)$$

For w(a), we take a triangular distribution rising linearly from $a_o - \Delta a$ to a_o and then falling linearly from a_o to $a_o + \Delta a$. (This is used here in preference to the usual gaussian because it imposes an upper and lower limit to a.) Eq. (17) represents the sum of independent scattering by the spheres and ignores the effect of inter-particle interference, but this is justified because in the Porod's region only the intra-particle scattering makes recognizable contribution.

The pin-hole collimation scattering curve I(s) is then obtained, according to eq. (1), by multiplying $I_{id}(s)$ with $H^2(s)$ to account for the diffuse boundaries and by adding I_b for the 'background.' Eq. (4), valid for the boundary profile obtainable under equilibrium conditions, is used for $H^2(s)$. I_b depends weakly on s, and its value extrapolated to s=0, for a pure amorphous material,

is given (Guinier 1963) by

$$I_b(0) = \rho^2 kT \kappa_T \tag{20}$$

where ρ is the electron density and κ_T the isothermal compressibility.

The following numerical values are used in the computation: $\Delta\rho = 4 \times 10^{-2}$ electrons/A^3, $f_1 = 0.25$, $a_o = 100A$, $\Delta a = 20A$, $I_b(0) = 0.3$ electrons^2/A^3. These are the values which would be found for example with styrene-butadiene block copolymers. Three different curves with boundary thickness t equal to 5, 20 and 40A are calculated.

The slit smearing effect is introduced, by means of eq. (5), into the pin-hole collimation intensity I(s) thus calculated. When the infinite-slit approximation is taken, $W_\ell(u)$ is a constant, which is here set arbitrarily equal to 0.5A. For the 'background' I_b, the infinite-slit approximation cannot be used. I_b and $\tilde{I}_b$ show about the same weak dependence on s, but their relative magnitudes depend on the actual slit weighting function $W_\ell(u)$. For the slit geometry typically encountered in Kratky cameras, $\tilde{I}_b/I_b \approx 0.05$ (when $W_\ell(0)$ is equated to 0.5A). Empirically, the angular dependence of $\tilde{I}_b$ was found (Vonk 1973, Todo, Hashimoto and Kawai 1978, Hashimoto, Shibayama and Kawai 1980) to obey the following relation fairly well

$$\tilde{I}_b = a + bs^n \tag{21}$$

with n an even integer. The following values of the constants are used in this work for the numerical calculation: a = 0.015 electron^2/A^3, b = 600 electron^{2}A and n = 4.

Finally, to simulate the counting statistical error, the exact

$\tilde{I}(s)$ values calculated at discrete s values are replaced by random numbers generated in accordance with gaussian statistics of the appropriate mean and variance. In the preset-time mode of data collection, or in the use of position-sensitive detectors, the variance of the error statistics is proportional to the intensity at each data point. The data points in the three constructed curves are given statistical errors accordingly, with their magnitudes adjusted to make the standard deviation at the lowest intensity point equal to 1%. The resulting three curves, for t = 5, 20 and 40A, are designated S1, S2 and S3 for later reference, and are shown in Fig. 2.

B. Single-phase structure

Single phase solutions, containing polymer molecules, can exhibit appreciable electron-density inhomogeneity due to concentration fluctuation and give rise to scattering of X-ray. The intensity can be especially pronounced when the structure is on the verge of phase transition. As a model scattering curve from such a system, we take the theoretical expression derived by Leibler (1980) for a homogeneous block copolymer system above the transition temperature of domain formation. The intensity of scattering given by eq. (IV-5) of his work depends on the parameters χ (the interaction parameter), R (the radius of gyration), N (the number of segments per molecule) and f (the fraction of component 1). To express the intensity in electron unit per unit volume, Leibler's expression has to be multiplied by $(\Delta\rho)^2 V_u$ where $\Delta\rho$ is the electron density difference between the components and V_u the volume of a polymer segment. The following numerical values for these parameters are chosen for computation: f = 0.25, R = 100A, N = 10^4, V_u = 10 A^3 and $\Delta\rho$ = 0.04 electrons/A^3. Two curves are constructed, one for XN = 17 and the other for χ = 0.

The second corresponds to a very high temperature and the first to a temperature just above the transition temperature.

Slit-smearing integration is then performed on these two curves, the 'background' $\tilde{I}_b$ is added, and the statistical errors are introduced, all in the same way as described in section A above. Fig. 3 shows the two curves finally obtained. They will be referred to as L1(XN = 17) and L2(X = 0).

IV. Error in the Evaluated Boundary Thickness

The method of determining the boundary thickness, described in Section II, is applied here to the synthesized scattering curves to see how well the original thickness values are recovered.

A. Effect of statistical error

Fig. 4 shows the plot of $\ln[(\tilde{I} - \tilde{I}_b)s^{1.8}]$ vs. s for the three synthesized curves S1, S2 and S3. The 'background' $\tilde{I}_b$ subtracted is the exact one which was initially added in the synthesis, i.e., that given by eq. (21) with a = 0.015, b = 600 and n = 4. The additional error which arises when a slightly erroneous $\tilde{I}_b$ is subtracted is to be examined later. Here the uncertainty in the value of t (or σ) determined arises solely because of the large scatter in the individual data points which becomes aggravated after the exact $\tilde{I}_b$ is subtracted. The angular range of data for which the slope can be evaluated is very limited, especially in the case of S3. The data in the low angle region deviates from Porod's law because of the interference effect reflecting the shape of the particles, while the high angle region cannot be used because of the excessive scatter of the points. The arrows in Fig. 4 indicate the range of s used for the evaluation of the slope. The boundary thickness calculated from the slope by eq. (14) is 8, 19 and 30 Å for S1, S2 and S3

respectively. These values are considerably different from the expected values 5, 20, and 40A. For curve S1, the angular range indicated in Fig. 1 corresponds to X = 0.7~1.3 when s is converted to x by eq. (9) with $\sigma(= \pi t/4\sqrt{3}) = 3.6$. The lower end of the x range thus extends slightly beyond the validity of the approximation given by eq. (12), and this partly explains why the t value obtained is too large. For S2 and S3 the error in t probably arises simply from the large uncertainty in the determination of the slope.

To see whether a substantially reduced statistical error in the data can lead to a more accurate value of the boundary thickness, additional scattering curves similar to S1, S2 and S3 are synthesized with 0.1%, instead of 1%, random counting error. The plots according to eq. (12) for these new curves are given in Fig. 5. Here the ranges of s at which the slope can be evaluated are wider and extend to larger angles. The evaluated t values are 6, 19 and 36A, which approach the true values much more closely. Even here, however, it would be difficult to claim an accuracy better than 10% in the determination of t.

B. Effect of erroneous background subtraction

In constructing the plots shown in Figs. 4 and 5, the same 'background' as originally added in the synthesis of the scattering curves was subtracted. In practice, however, the 'background' has to be estimated from analysis of high angle data. Error in the estimated background can arise not only because of the scatter in the data, but also because the valid analytical form for the background intensity curve is usually not known. Several workers (Vonk 1973; Todo, Hashimoto and Kawai 1978; Hashimoto, Shibayama and Kawai 1980; Roe, Fishkis and Chang 1981) found the empirical eq. (21)

to fit the observed background fairly well, while Rathje and Ruland (1976) and Wiegand and Ruland (1979) used the exponential form

$$\tilde{I}_b = a \exp(bs^2). \tag{22}$$

Among the four possible analytical forms, i.e., eq. (21) with n = 2, 4 and 6 and eq. (22), more than one may give apparently satisfactory fit to the data within the error. The somewhat arbitrary choice of the analytical form can then influence the value of the boundary thickness finally evaluated.

In the synthesis of curves S1, S2 and S3, the background was added by eq. (21) with n = 4. Fig. 6 gives the plot of these scattering curves against s^6 as the abscissa, and shows that eq. (21) with n = 6 is a fairly satisfactory approximation. Here the data extends up to s = 0.05. After the backgrounds evaluated according to the straight lines drawn in Fig. 6 are subtracted from S1, S2 and S3, the plots of $\ln[(\tilde{I} - \tilde{I}_b)s^{1.8}]$ against s are constructed in Fig. 7. The boundary thicknesses evaluated from the slopes are 12, 22 and 49A, respectively all substantially exceeding the true values 5, 20 and 40A.

In Fig. 8 curves S1, S2 and S3 are replotted to show that eq. (22) is also a reasonably good approximation. Here again s extends up to 0.05. After subtraction of the background given by the straight lines in Fig. 8, the plots to evaluate the boundary thickness are constructed in Fig. 9, from which extremely erroneous t values of 8, 11 and 9A are obtained for S1, S2 and S3, respectively.

There are some latitudes in the values of a and b which are determined from such plots as given in Figs. 6 and 8. The boundary thickness values finally evaluated are less sensitive to the uncertainties in these constants, and are found to vary less than

10% in most cases. This fact probably led to the occasional statements in the literature that the boundary thickness values determined were not very sensitive to the method of background subtraction.

C. Illusory boundary thickness in a single phase structure

An experimental scattering curve from a specimen which does not contain a two phase structure may nevertheless sometimes yield an illusory boundary thickness if the procedure is blindly applied to it. The scattering curves synthesized in Section IIIB, on the basis of the theory by Leibler (1980) of a homogeneous (single-phase) block copolymer, are utilized here to examine this possibility.

Fig. 10 shows the two curves L1 and L2 plotted against s^4, to evaluate the background in accordance with eq. (21) with n = 4. The values of the constants a and b in eq. (21) obtained from Fig. 10 are 0.0196 and 280, respectively, which are appreciably different from 0.015 and 600 used in the synthesis of these curves initially. The component of scattering due to concentration fluctuation decays rather slowly with s, and some of it is erroneously included in the background evaluated in the above manner. The erroneous background is subtracted from L1 and L2 and Fig. 11 shows the plot constructed for the determination of the boundary thickness in the usual manner. Quite possibly one could be misled to taking the slope as given by the straight line there and come to the conclusion that t is equal to around 10A.

V. Discussion

The numerical examples given in the previous section demonstrate that under favorable conditions the boundary thickness t can

be evaluated correctly. They also point out the need to guard against the possibility of obtaining seriously erroneous results.

As discussed in the introduction, the basic problem is that the two types of deviations from Porod's law due to the diffuse boundary and the density fluctuation produce opposite effects, which can be separated from each other only with difficulty. As the numerical examples in Section IIIB illustrate, assumption of wrong analytical forms for the background intensity can lead to grossly misleading values of the boundary thickness. The danger of the wrong background equation can be alleviated by extending the collection of the data to higher angles. This may not eliminate it completely, however, since there is never a guarantee that an empirical equation giving a good fit at high angles is indeed a valid one in the low angle region of importance for the boundary thickness determination. If each of the components forming the two phase structure can be obtained in pure form, more reliable background can be obtained by measuring the scattering from the pure materials separately and calculating the weighted average of the two.

The statistical error of counting present in the data makes the evaluation of the thickness doubly difficult. First, it makes the separation of the background uncertain. Second, even when the background can be subtracted correctly, the scatter in the data reduces the precision of the obtained t value markedly. The examples given in Section IIIA show that a statistical error corresponding to 1% standard deviation in the background region is barely tolerable, if an accuracy in t better than 20% is desired. One should probably aim at achieving a statistical error of less than 0.1% in the background -- an aim which may not easily be

attained in practice. To accumulate 10^6 counts per channel in the background with amorphous polymers, it may take several days with a Kratky camera fitted with a one-dimensional position sensitive detector and operating on a rotating anode tube. Accumulation of such high counts, for only a few samples, may also alter the detection efficiency characteristics of the position-sensitive detector (Roe, Chang, Fishkis and Curro 1981) noticably. An important factor affecting the error in t is the relative magnitudes of the Porod Law intensity and the background intensity. Collimation with a long slit will increase the latter more than the former, and therefore short slit or pin-hole collimation would be advantageous under otherwise comparable conditions.

The conclusions derived in this work are based on numerical results obtained with synthesized scattering curves. Although they are constructed to model typical experimental curves in realistic detail, there would of course be experimental results which differ greatly from them. In such cases the assessment of the error given in this work may not be exactly valid. One may then be required to undertake an assessment of the error in the evaluated boundary thickness by repeating what is described in this work, that is, by synthesizing a scattering curve embodying the structure under study and the slit geometry used and by examining how well the boundary thickness built into the scattering curve can be recovered.

Acknowledgment

This work was supported in part by the Office of Naval Research.

References

Cahn, J. W. and Hilliard, J. E. (1958). J. Chem. Phys., 28, 258.

Guinier, A. (1963). "X-ray Diffraction," Freeman and Co., San Francisco.

Hashimoto, T., Shibayama, M. and Kawai, H. (1980). Macromolecules, 13, 1237.

Hashimoto, T., Todo, A., Itoi, H. and Kawai, H. (1977). Macromolecules, 10, 377.

Helfand, E. (1975). Acc. Chem. Res., 8, 295.

Helfand, E. and Tagami, Y. (1971). Polym. Lett., 9, 741.

Hopper, R. W. and Uhlmann, D. R. (1974). J. Colloid Interface Sci., 47, 77.

Koberstein, J. T., Morra, B. and Stein, R. S. (1980). J. Appl. Cryst., 13, 34.

Leibler, L. (1980). Macromolecules, 13, 1602.

Porod, G. (1951). Kolloid-Z., 124(2), 83.

Porod, G. (1952a). Kolloid-Z., 125(1), 51.

Porod, G. (1952b). Kolloid-Z., 125(2), 108.

Rathje, J. and Ruland, W. (1976). Colloid Polym. Sci., 254, 358.

Roe, R. J. (1975). J. Chem. Phys., 62, 490.

Roe, R. J., Chang, J. C., Fishkis, M. and Curro, J. J. (1981). J. Appl. Cryst., 14, 139.

Roe, R. J., Fishkis, M. and Chang, J. C. (1981). Macromolecules in press.

Ruland, W. (1971). J. Appl. Cryst., 4, 70.

Ruland, W. (1974). J. Appl. Cryst., 7, 383.

Ruland, W. (1980). Abstract of papers presented at the Symposium on Small-Angle X-ray and Neutron Scattering in Strasbourg, France, p. 78.

Todo, A., Hashimoto, T. and Kawai, H. (1978). J. Appl. Cryst., 11, 558.

Vonk, C. G. (1973). J. Appl. Cryst., 6, 81.

Wiegand, W. and Ruland, W. (1979). Progr. Colloid Polym. Sci., 66, 355.

Legend to Figures

Fig. 1. The plot illustrates that eq. (12) approximates $\tilde{g}(x)$ well for x between 0.8 and 6.0. Here $\tilde{g}(x)$, given by eqs. (10) and (11), is the function representing the Porod's law intensity for structures having diffuse boundary in the case of infinite-slit geometry.

Fig. 2. The plots show the synthesized scattering curves which simulate the SAXS patterns obtainable with infinite-slit collimation from samples containing spherical domains (with a triangular distribution of the radius between 80 and 120A) imbedded in a continuous matrix of another phase. The background intensity in the form $a+bs^4$ is assumed. Curves S1, S2, and S3 are for the boundary thicknesses of 5, 20 and 40A respectively. The statistical error added corresponds to 1% standard deviation at the point of lowest intensity.

Fig. 3. The plots show the synthesized scattering curves, which simulate the SAXS pattern obtainable with infinite slit collimation from a sample containing a homogeneous, single-phase block copolymer. The theoretical equation derived by Leibler (1980) is utilized, but the background ($a+bs^4$), slit-smearing and statistical errors are also added. L1 is for $\chi N = 17$ and L2 for $\chi N = 0$.

Fig. 4. Curves S1, S2 and S3 are plotted in accordance with the method described in Section II for evaluation of boundary thickness. (For the sake of legibility, the plots for S2 and S3 are displaced downward by multiplication of 0.1 and 0.01 respectively.) The exact background, as was initially added in the construction of the synthesized curves, was

subtracted from them before making the plot. The range of s at which the slope is evaluated is indicated by arrows. The thickness t obtained is 8, 19 and 30A for S1, S2 and S3, respectively.

Fig. 5. These plots are similar to those shown in Fig. 4, except that the curves S1′, S2′, and S3′ shown here are ones constructed with statistical errors corresponding to 0.1% at the lowest intensity data point. The much smaller scatter enables the slope to be evaluated in wider ranges of s extending into larger angles. The thickness values evaluated 6, 19 and 36A now agree better with the true values.

Fig. 6. The plots illustrate that a reasonably good approximation to the background can be obtained even when a wrong analytical equation ($a+bs^6$, instead of the correct one $a+bs^4$) is assumed. The plots for S2 and S3 are displaced downward for legibility by subtraction of a constant term 0.01 and 0.02 respectively.

Fig. 7. The erroneous backgrounds, evaluated according to Fig. 6, were subtracted from the scattering curves S1, S2 and S3, before constructing the plot to evaluate the boundary thickness. (The plots for S2 and S3 are displaced downward for legibility.) The thickness t, evaluated from the slopes indicated by the straight lines drawn, are 12, 22 and 49A for the three curves respectively, all larger than the true values.

Fig. 8. The plots illustrate that the background, originally synthesized according to $a+bs^4$, can be fitted fairly well by $a\exp(bs^2)$. (The plots for S2 and S3 are displaced downward for legibility by multiplying by 0.5 and 0.25 respectively.)

Fig. 9. The erroneous backgrounds, evaluated according to Fig. 8, were subtracted from the scattering curves S1, S2 and S3, before constructing the plot to evaluate the boundary thickness. (The plots for S2 and S3 are displaced downward for legibility). The thickness t, evaluated from the slopes indicated by the straight lines drawn, are 8, 11 and 9A respectively, the latter two being grossly in error.

Fig. 10. The single-phase scattering curves L1 and L2 were originally synthesized with the background $0.015+600s^4$. The plots shown here illustrate that, despite the correct equation with a 4th order term assumed for the background, the best fit obtained differs greatly and is given by $0.020+280s^4$. (The plot for L2 is displaced downward by 0.01 for legibility.)

Fig. 11. The single-phase scattering curves L1 and L2, from which the erroneous backgrounds evaluated in Fig. 10 were subtracted, are plotted according to the method to be used for evaluation of the boundary thickness. (The plot for L2 is displaced downward by multiplication of a factor 0.1.) The downward trend of the data points at high angles, produced by subtraction of the incorrect background, can erroneously be interpreted to mean the presence of phase boundary of thickness 11A.

Fig. 1

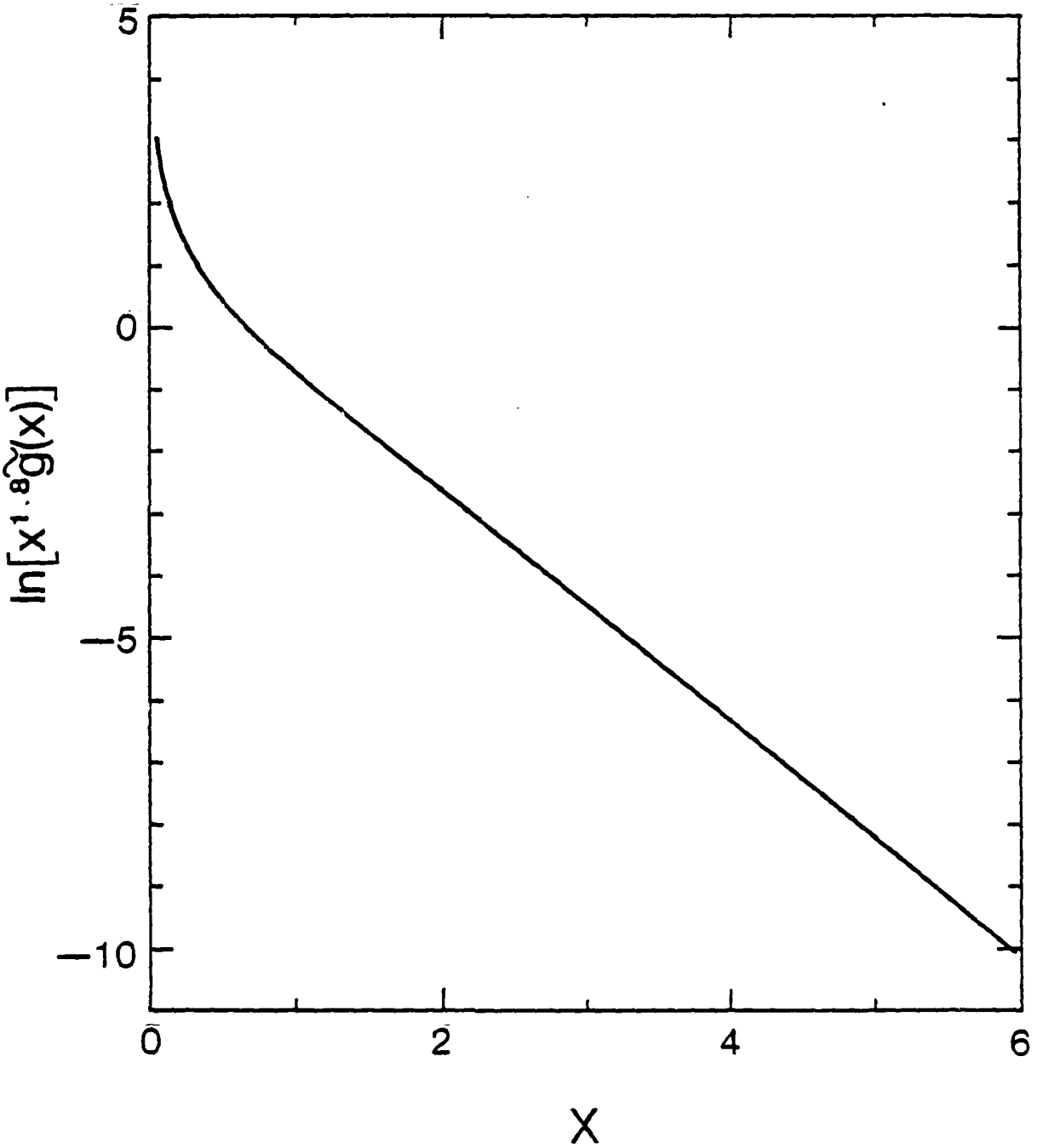

Fig. 2

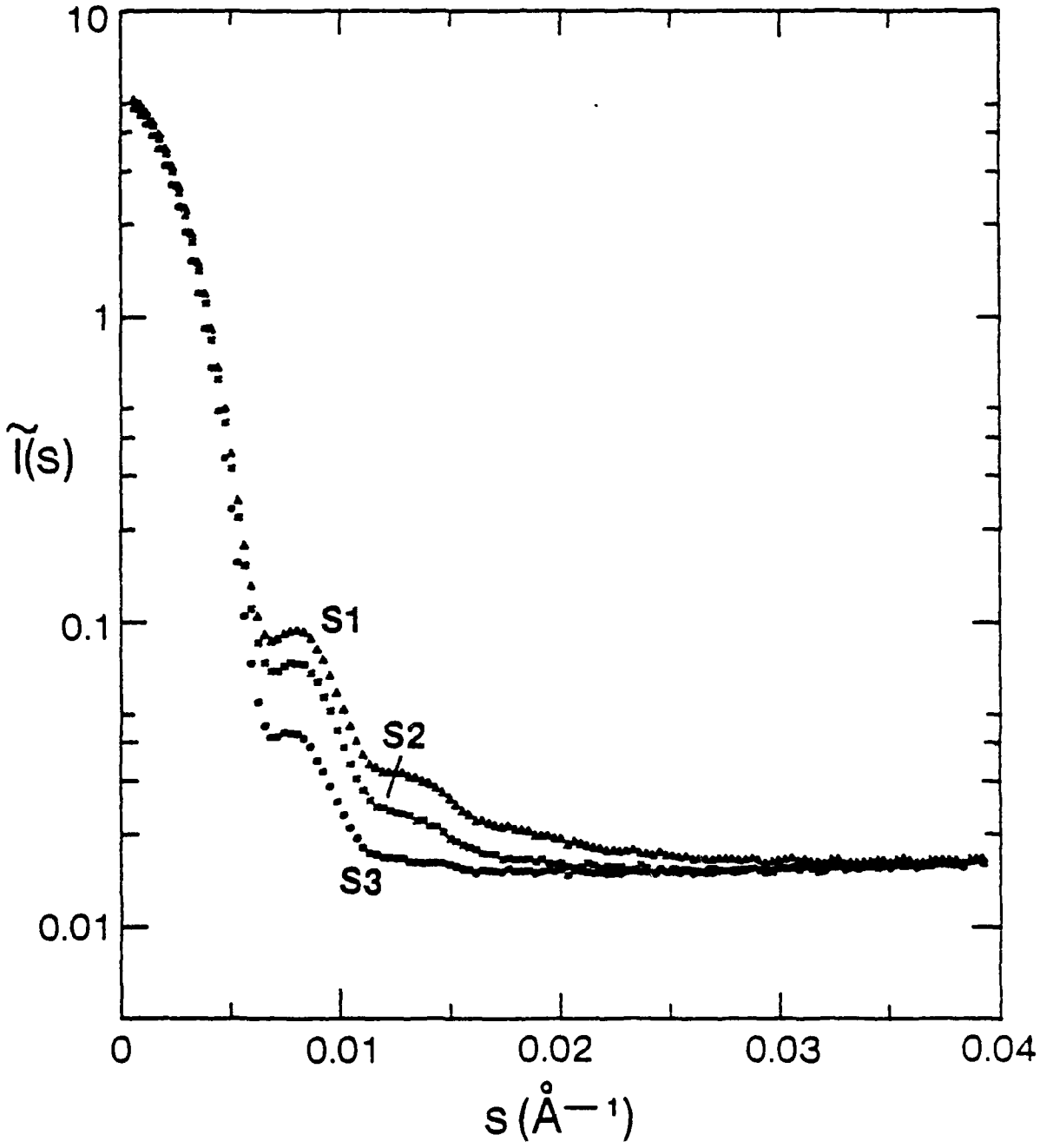

Fig. 3

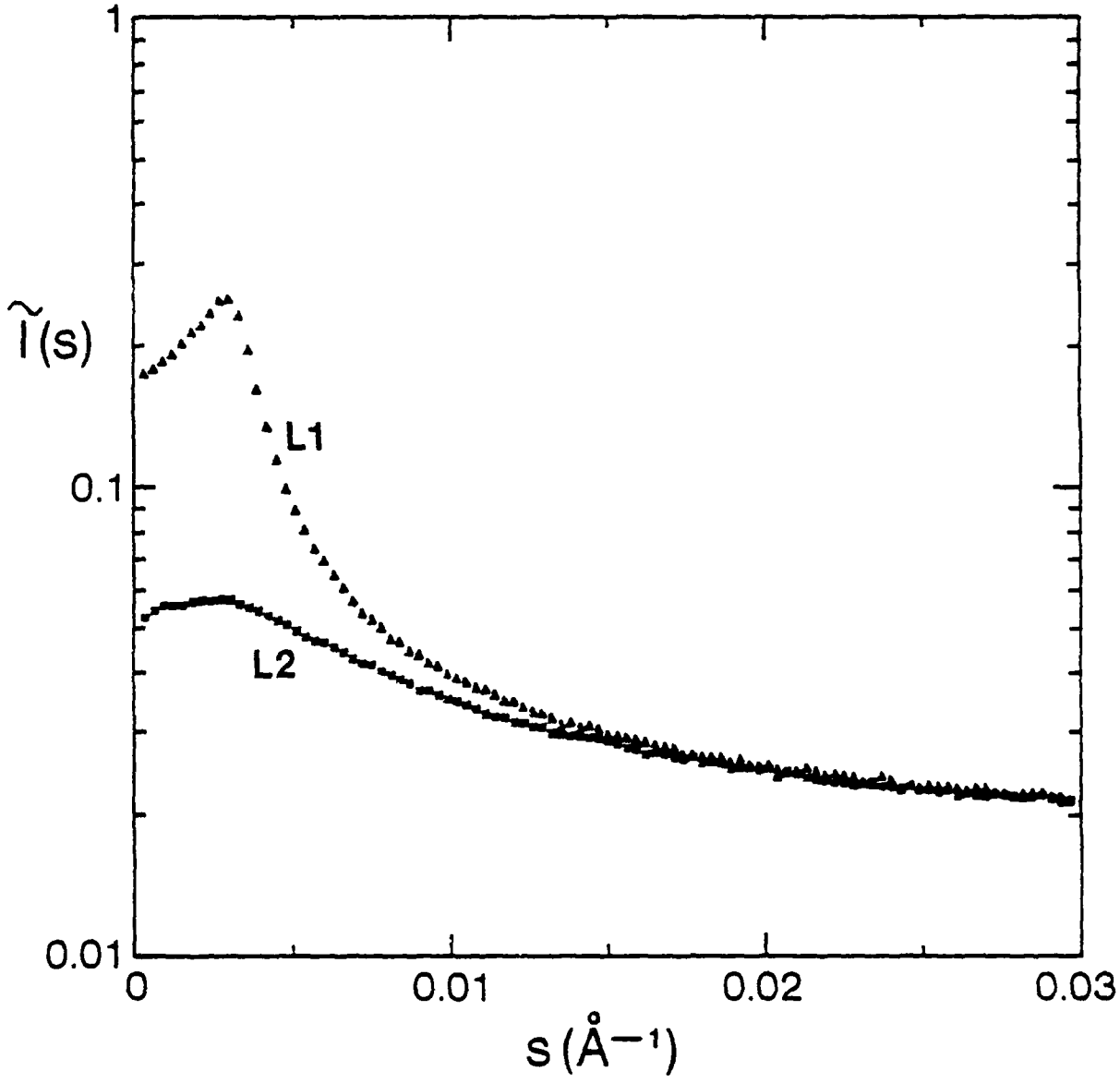

Fig. 4

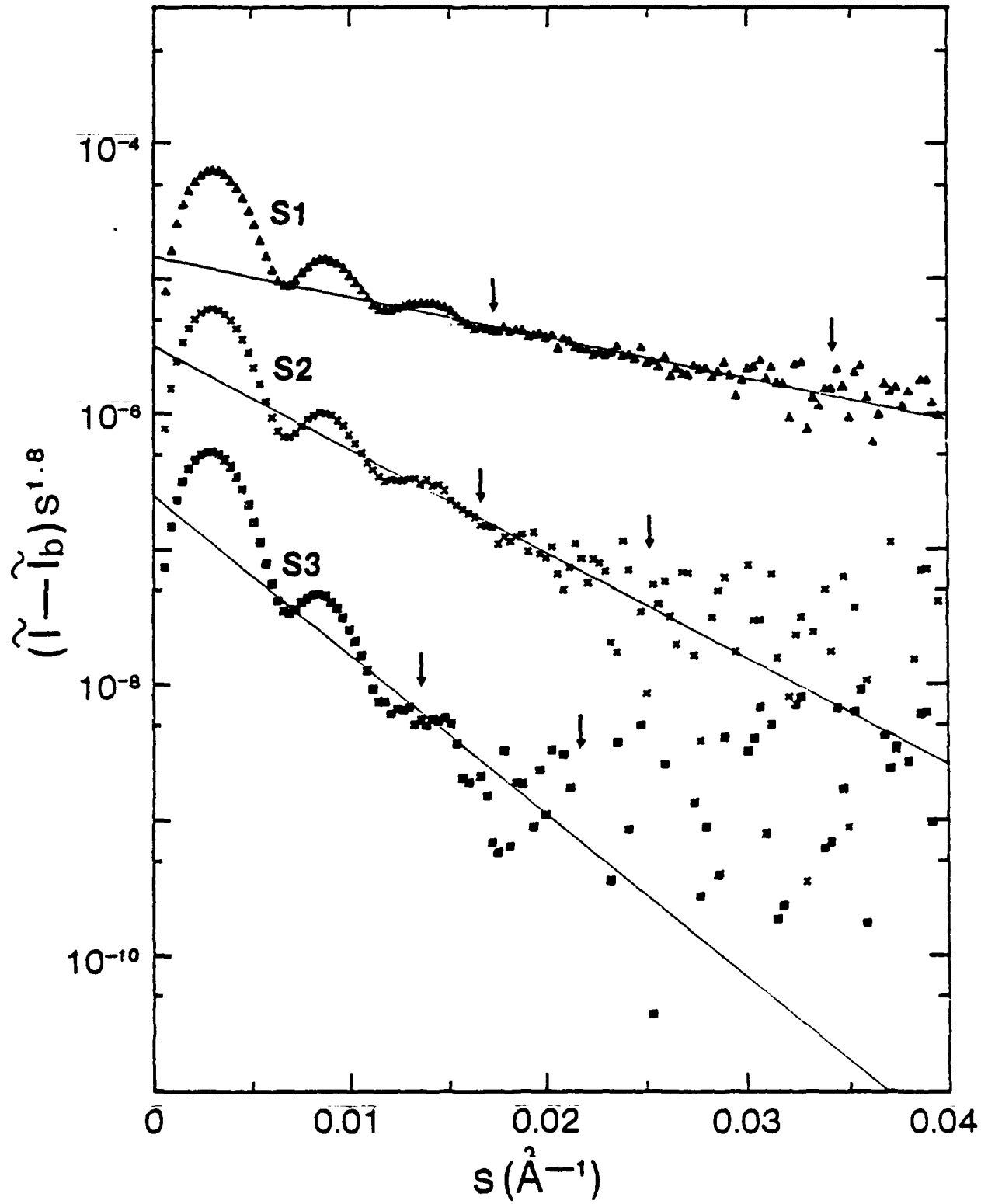
S1
S2
S3
10^{-4}
10^{-6}
10^{-8}
10^{-10}
$(\tilde{I} - \tilde{I}_b) s^{1.8}$
0
0.01
0.02
0.03
0.04
s (Å^{-1})

Fig.5

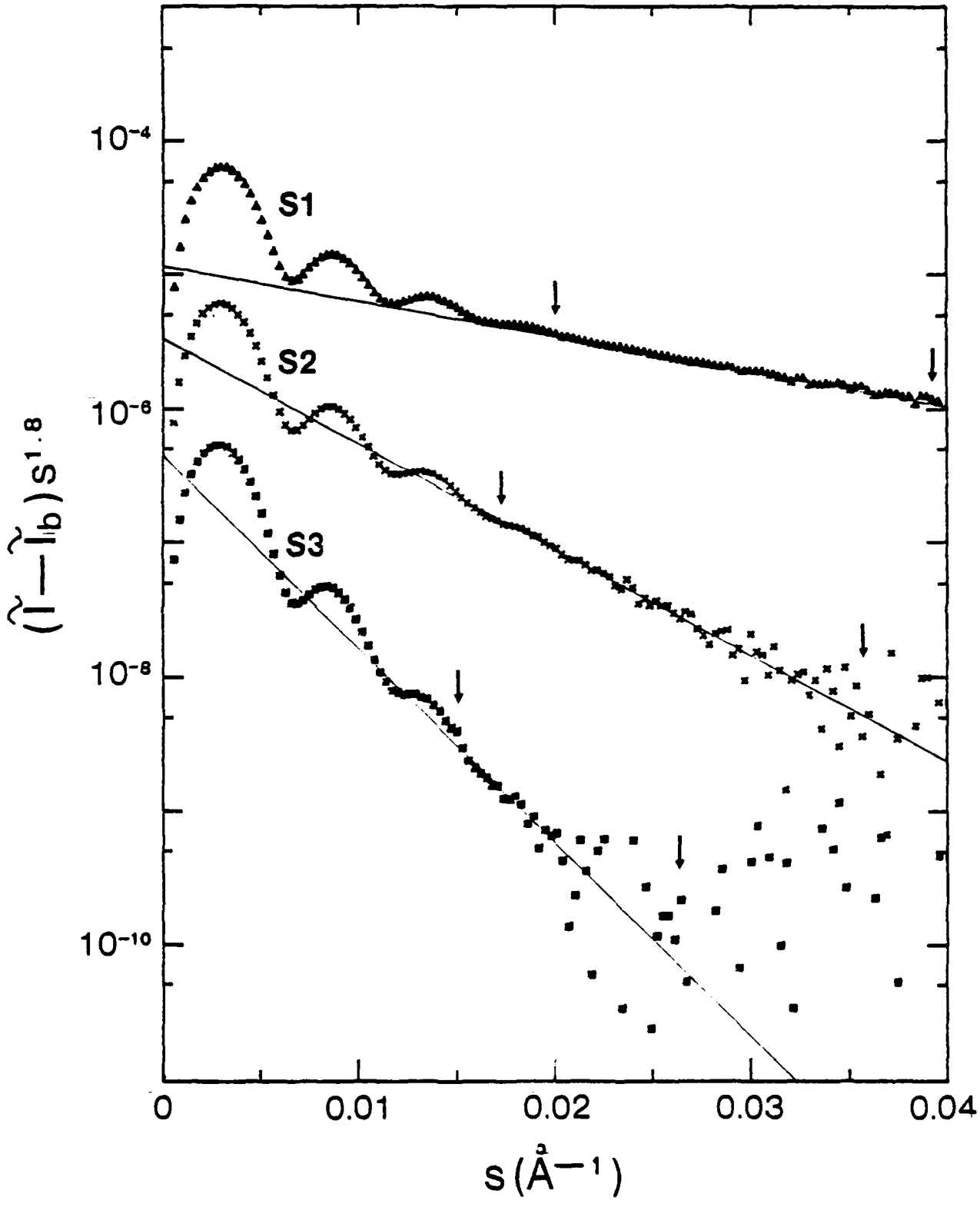
S1
S2
S3
10^{-4}
10^{-6}
10^{-8}
10^{-10}
$(\tilde{I} - \tilde{I}_b)s^{1.8}$
0
0.01
0.02
0.03
0.04
s (Å^{-1})

Fig. 6

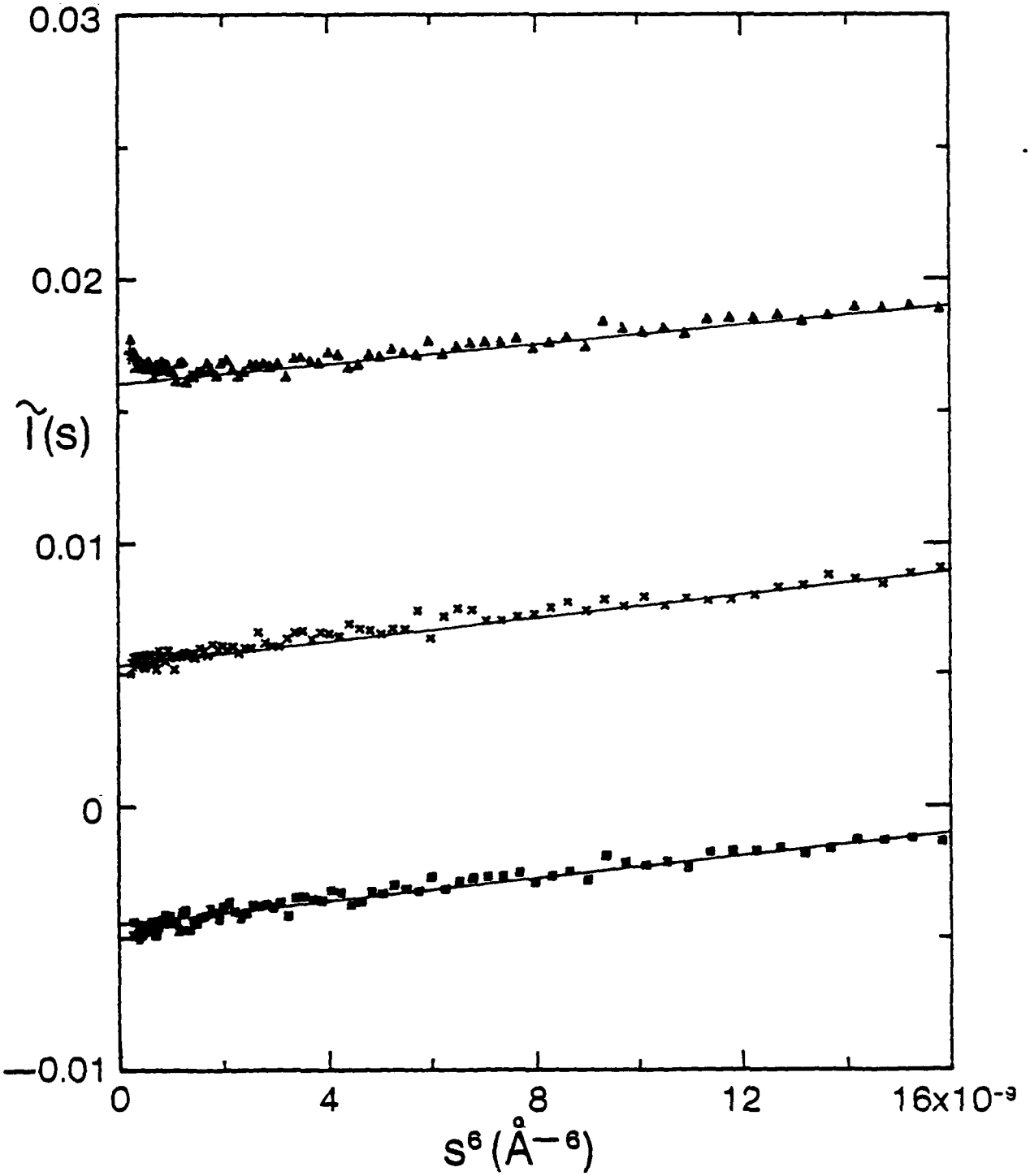

Fig. 7

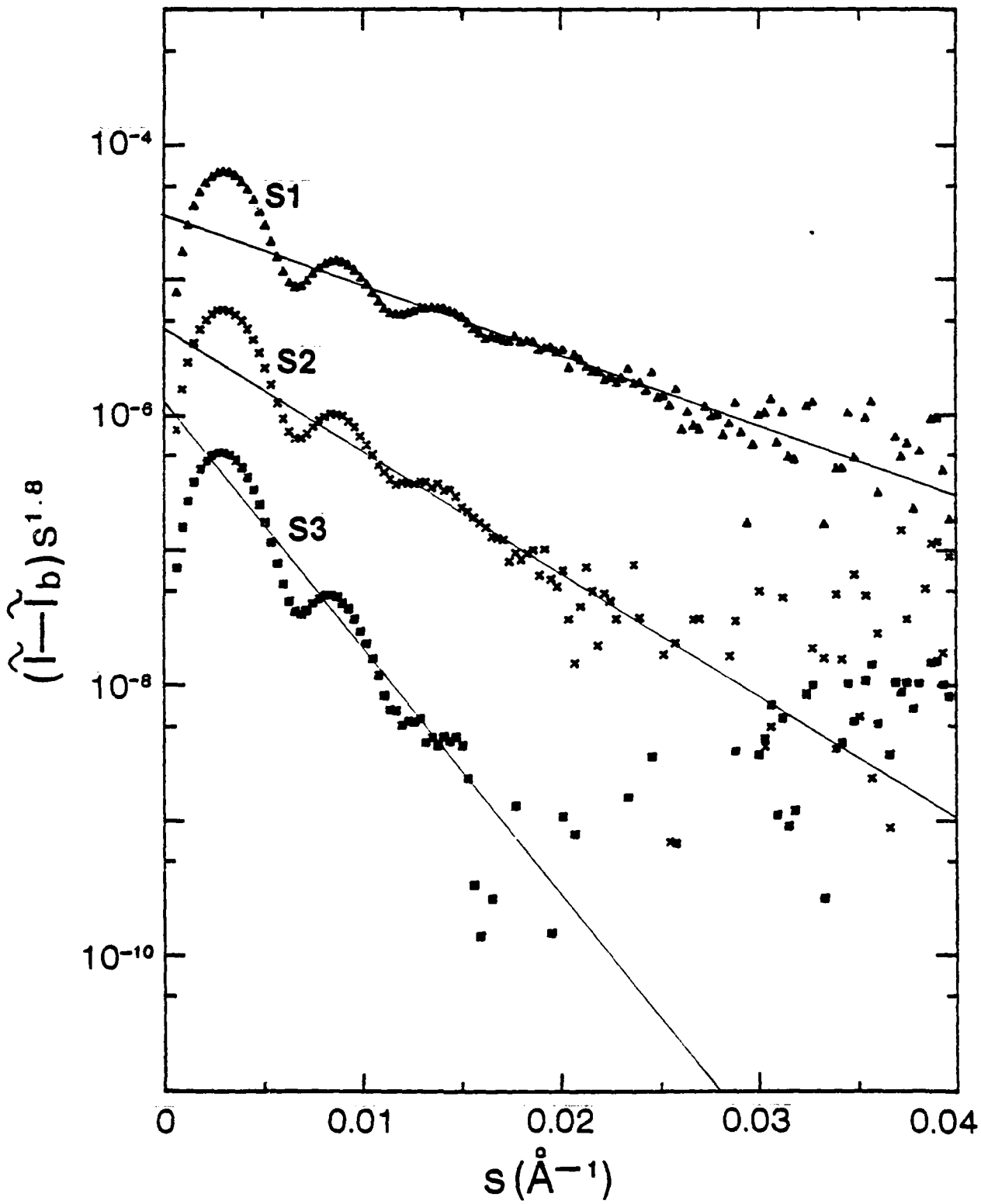
S1
S2
S3
10^{-4}
10^{-6}
10^{-8}
10^{-10}
$(\tilde{I} - \tilde{I}_b)s^{1.8}$
0
0.01
0.02
0.03
0.04
s (Å^{-1})

Fig. 8

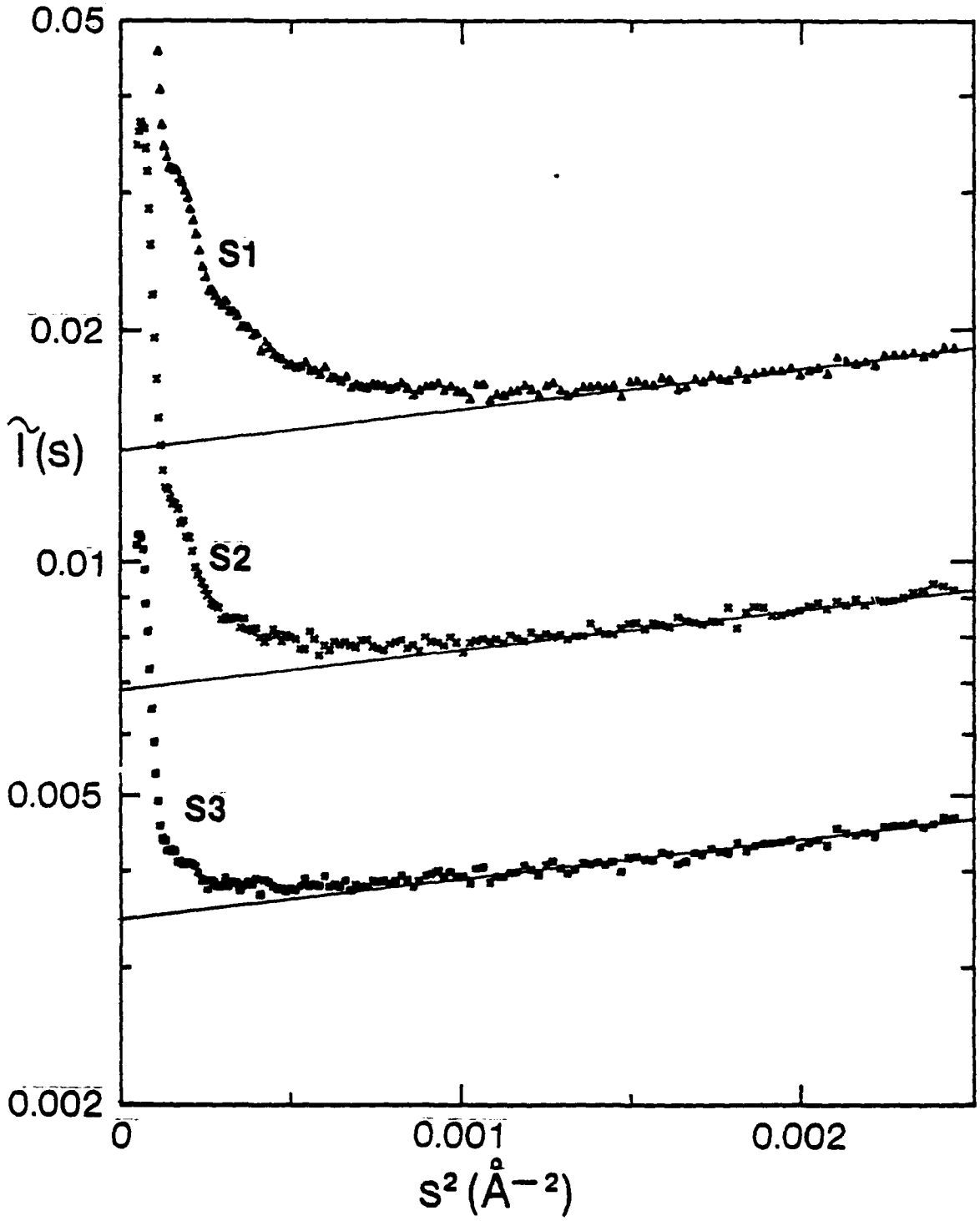

Fig. 9

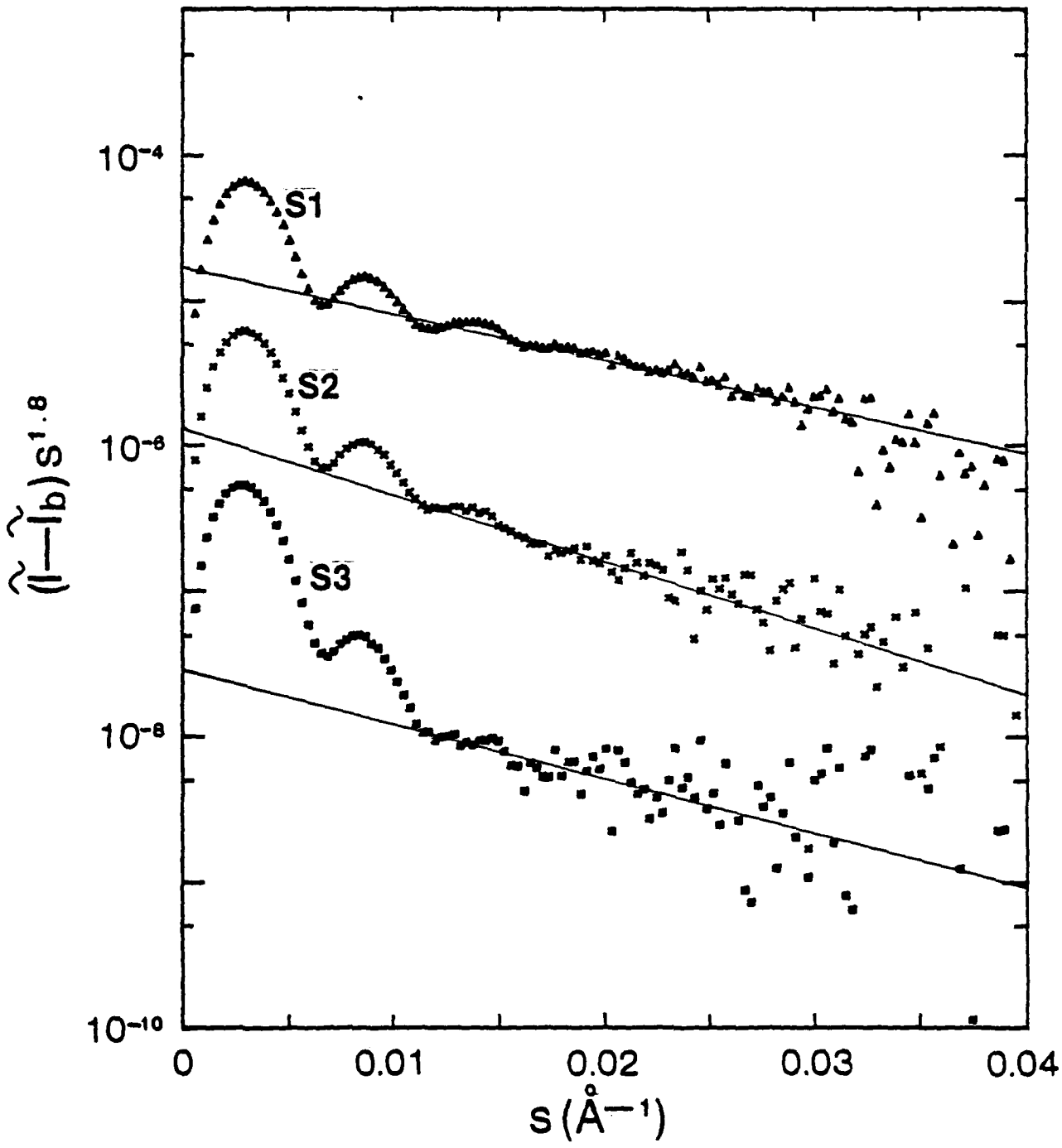
S1
S2
S3
10^{-4}
10^{-6}
10^{-8}
10^{-10}
$(\tilde{I} - \tilde{I}_b)\, s^{1.8}$
0
0.01
0.02
0.03
0.04
s (Å^{-1})

Fig. 10

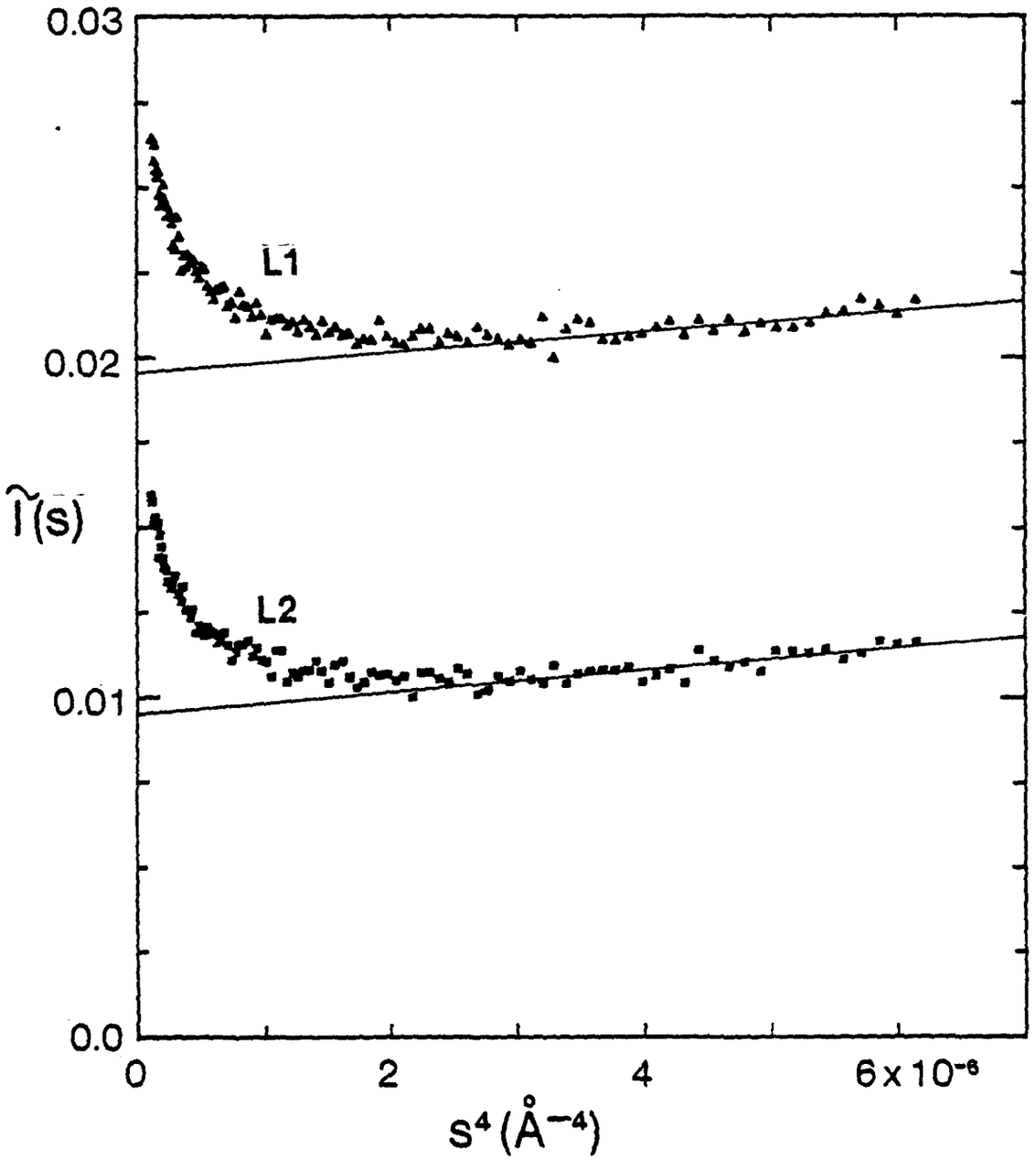

Fig. 11

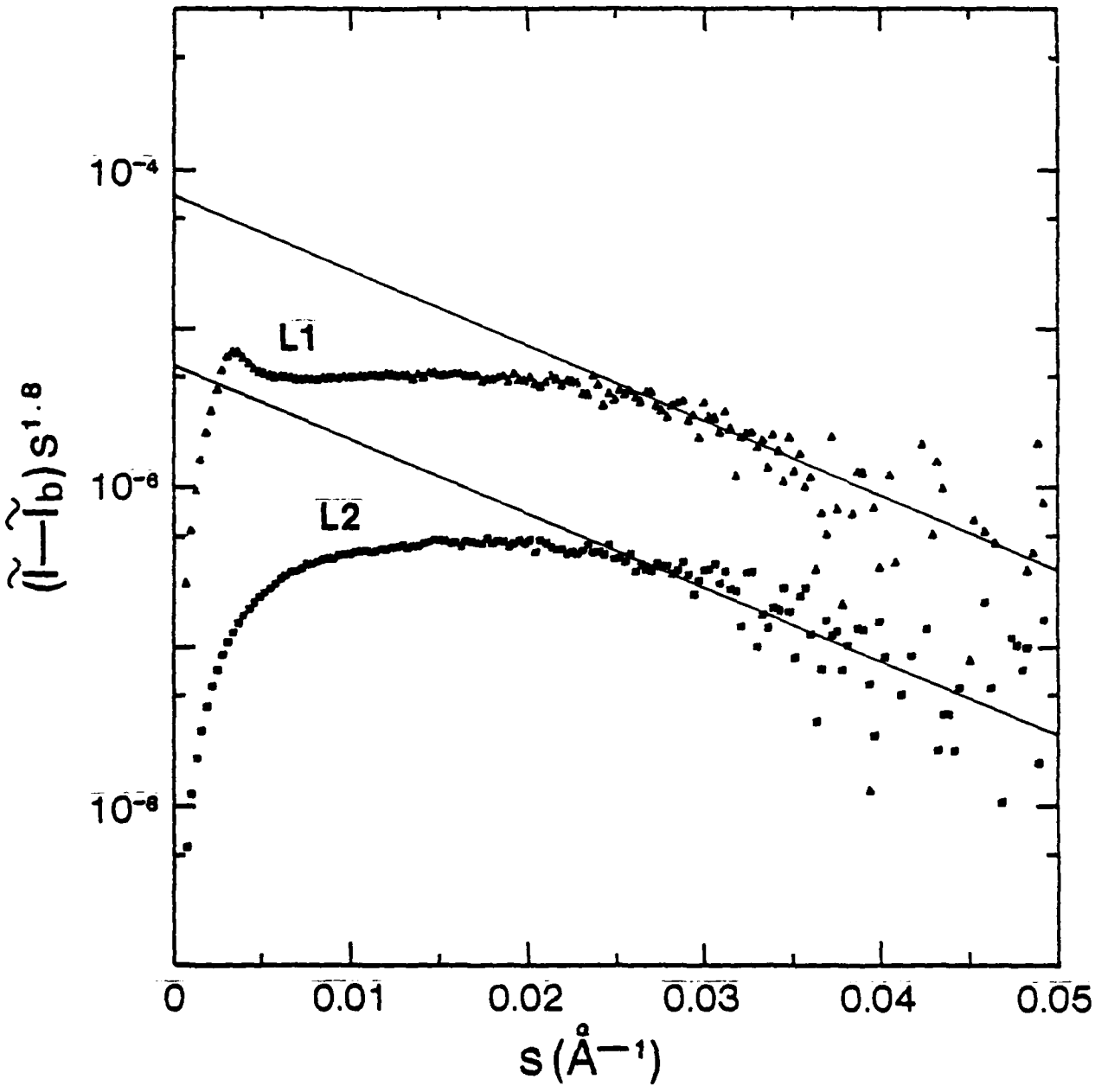

TECHNICAL REPORT DISTRIBUTION LIST, GEN

	No. Copies
Office of Naval Research Attn: Code 472 800 North Quincy Street Arlington, Virginia 22217	2
ONR Branch Office Attn: Dr. George Sandoz 536 S. Clark Street Chicago, Illinois 60605	1
~~ONR Area Office Attn: Scientific Dept. 715 Broadway New York, New York 10003~~	1
ONR Western Regional Office 1030 East Green Street Pasadena, California 91106	1
ONR Eastern/Central Regional Office Attn: Dr. L. H. Peebles Building 114, Section D 666 Summer Street Boston, Massachusetts 02210	1
Director, Naval Research Laboratory Attn: Code 6100 Washington, D.C. 20390	1
The Assistant Secretary of the Navy (RE&S) Department of the Navy Room 4E736, Pentagon Washington, D.C. 20350	1
Commander, Naval Air Systems Command Attn: Code 310C (H. Rosenwasser) Department of the Navy Washington, D.C. 20360	1
Defense Technical Information Center Building 5, Cameron Station Alexandria, Virginia 22314	12
Dr. Fred Saalfeld Chemistry Division, Code 6100 Naval Research Laboratory Washington, D.C. 20375	1

	No. Copies
U.S. Army Research Office Attn: CRD-AA-IP P.O. Box 1211 Research Triangle Park, N.C. 27709	1
Naval Ocean Systems Center Attn: Mr. Joe McCartney San Diego, California 92152	1
Naval Weapons Center Attn: Dr. A. B. Amster, Chemistry Division China Lake, California 93555	1
Naval Civil Engineering Laboratory Attn: Dr. R. W. Drisko Port Hueneme, California 93401	1
Department of Physics & Chemistry Naval Postgraduate School Monterey, California 93940	1
Dr. A. L. Slafkosky Scientific Advisor Commandant of the Marine Corps (Code RD-1) Washington, D.C. 20380	1
Office of Naval Research Attn: Dr. Richard S. Miller 800 N. Quincy Street Arlington, Virginia 22217	1
Naval Ship Research and Development Center Attn: Dr. G. Bosmajian, Applied Chemistry Division Annapolis, Maryland 21401	1
Naval Ocean Systems Center Attn: Dr. S. Yamamoto, Marine Sciences Division San Diego, California 91232	1
Mr. John Boyle Materials Branch Naval Ship Engineering Center Philadelphia, Pennsylvania 19112	1

TECHNICAL REPORT DISTRIBUTION LIST, GEN

	No. Copies
Dr. Rudolph J. Marcus Office of Naval Research Scientific Liaison Group American Embassy APO San Francisco 96503	1
Mr. James Kelley DTNSRDC Code 2803 Annapolis, Maryland 21402	1

TECHNICAL REPORT DISTRIBUTION LIST, 356A

	No. Copies
Mr. Robert W. Jones Advanced Projects Manager Hughes Aircraft Company Mail Station D 132 Culver City, California 90230	1
Dr. C. Giori IIT Research Institute 10 West 35 Street Chicago, Illinois 60616	1
Dr. M. Litt Department of Macromolecular Science Case Western Reserve University Cleveland, Ohio 44106	1
~~Dr. R. S. Roe Department of of Materials Science and Metallurgical Engineering University of Cincinnati Cincinnati, Ohio 45221~~	1
Dr. Robert E. Cohen Chemical Engineering Department Massachusetts Institute of Technology Cambridge, Massachusetts 02139	1
Dr. T. P. Conlon, Jr., Code 3622 Sandia Laboratories Sandia Corporation Albuquerque, New Mexico	1
Dr. Martin Kaufmann, Head Materials Research Branch, Code 4542 Naval Weapons Center China Lake, California 93555	1
Professor S. Senturia Department of Electrical Engineering Massachusetts Institute of Technology Cambridge, Massachusetts 02139	1
Dr. T. J. Reinhart, Jr., Chief Composite and Fibrous Materials Branch Nonmetallic Materials Division Department of the Air Force Air Force Materials Laboratory (AFSC) Wright-Patterson AFB, Ohio 45433	1
Dr. J. Lando Department of Macromolecular Science Case Western Reserve University Cleveland, Ohio 44106	1
Dr. J. White Chemical and Metallurgical Engineering University of Tennessee Knoxville, Tennessee 37916	1
Dr. J. A. Manson Materials Research Center Lehigh University Bethlehem, Pennsylvania 18015	1
Dr. R. F. Helmreich Contract RD&E Dow Chemical Co. Midland, Michigan 48640	1
Dr. R. S. Porter Department of Polymer Science and Engineering University of Massachusetts Amherst, Massachusetts 01002	1
Professor Garth Wilkes Department of Chemical Engineering Virginia Polytechnic Institute and State University Blacksburg, Virginia 24061	1
Dr. Kurt Baum Fluorochem Inc. 6233 North Irwindale Avenue Azuza, California 91702	1
Professor C. S. Paik Sung Department of Materials Sciences and Engineering Room 8-109 Massachusetts Institute of Technology Cambridge, Massachusetts 02139	1

TECHNICAL REPORT DISTRIBUTION LIST, 356A

	No. Copies
Dr. Stephen H. Carr Department of Materials Science Northwestern University Evanston, Illinois 60201	1
Dr. M. Broadhurst Bulk Properties Section National Bureau of Standards U.S. Department of Commerce Washington, D.C. 20234	2
Professor G. Whitesides Department of Chemistry Massachusetts Institute of Technology Cambridge, Massachusetts 02139	1
Professor J. Wang Department of Chemistry University of Utah Salt Lake City, Utah 84112	1
Dr. V. Stannett Department of Chemical Engineering North Carolina State University Raleigh, North Carolina 27607	1
Dr. D. R. Uhlmann Department of Metallurgy and Material Science Massachusetts Institute of Technology Cambridge, Massachusetts 02139	1
Naval Surface Weapons Center Attn: Dr. J. M. Augl, Dr. B. Hartman White Oak Silver Spring, Maryland 20910	1
Dr. G. Goodman Globe Union Incorporated 5757 North Green Bay Avenue Milwaukee, Wisconsin 53201	1
Professor Hatsuo Ishida Department of Macromolecular Science Case-Western Reserve University Cleveland, Ohio 44106	1
Picatinny Arsenal Attn: A. M. Anzalone, Building 3401 SMUPA-FR-M-D Dover, New Jersey 07801	1
Dr. J. K. Gillham Department of Chemistry Princeton University Princeton, New Jersey 08540	1
Douglas Aircraft Co. Attn: Technical Library Cl 290/36-84 AUTO-Sutton 3855 Lakewood Boulevard Long Beach, California 90846	1
Dr. E. Baer Department of Macromolecular Science Case Western Reserve University Cleveland, Ohio 44106	1
Dr. K. D. Pae Department of Mechanics and Materials Science Rutgers University New Brunswick, New Jersey 08903	1
NASA-Lewis Research Center Attn: Dr. T. T. Serofini, MS-49-1 21000 Brookpark Road Cleveland, Ohio 44135	1
Dr. Charles H. Sherman Code TD 121 Naval Underwater Systems Center New London, Connecticut	1
Dr. William Risen Department of Chemistry Brown University Providence, Rhode Island 02192	1
Dr. Alan Gent Department of Physics University of Akron Akron, Ohio 44304	1

DATE
FILMED

7-8